JPE 16-1-29

http://dx.doi.org/10.6113/JPE.2016.16.1.277
ISSN(Print): 1598-2092 / ISSN(Online): 2093-4718

Novel Predictive Maximum Power Point Tracking Techniques for Photovoltaic Applications

Omar Abdel-Rahim[*,†], Hirohito Funato[*], and Junnosuke Haruna[*]

[*]Dept. of Electrical and Electronic Eng., Utsunomiya University, Utsunomiya, Japan
[†]Dept. of Electrical Eng., Aswan University, Aswan, Egypt

Abstract

This paper offers two Maximum Power Point Tracking (MPPT) systems for Photovoltaic (PV) applications. The first MPPT method is based on a fixed frequency Model Predictive Control (MPC). The second MPPT technique is based on the Predictive Hysteresis Control (PHC). An experimental demonstration shows that the proposed techniques are fast, accurate and robust in tracking the maximum power under different environmental conditions. A DC/DC converter with a high voltage gain is obligatory to track PV applications at the maximum power and to boost a low voltage to a higher voltage level. For this purpose, a high gain Switched Inductor Quadratic Boost Converter (SIQBC) for PV applications is presented in this paper. The proposed converter has a higher gain than the other transformerless topologies in the literature. It is shown that at a high gain the proposed SIQBC has moderate efficiency.

Key words: Maximum Power Point Tracking, Photovoltaic, Model Predictive Control, Predictive Hysteresis Control, Switched Inductor Quadratic Boost Converter

I. INTRODUCTION

Driven by anxieties over environmental protection and energy accessibility, the installation of photovoltaic (PV) energy-productions systems has been noticeably enlarged during the last years. The decreasing prices of PV modules and more highly efficient power conversion systems have supported that trend by augmenting the economic viability of the installed PV systems. More than 38 GW of new PV capacity was installed across the world during 2013, which resulted in a worldwide cumulative installed capacity of 138.9 GW during that year [1], [2]. A simple microgrid consists of at least one distributed generation source, a load, and storage systems [3]-[6]. Renewable energies like solar and wind are environmentally friendly sustainable sources of energy [7]-[13]. One of the most efficient and well-accepted renewable energy source is Photovoltaic (PV) systems. Adequate and efficient Maximum Power Point Tracking (MPPT) is needed, due to the nonlinearity of PV sources. Several techniques have been proposed for maximum power tracking [7]-[20]. MPPT algorithms have to be stable, robust, fast, and efficient. Due to fast changes in environmental conditions, MPPT algorithms should respond quickly to changes in atmospheric conditions. The Perturb and Observe (P&O) method is one of the most commonly used techniques, due to its simplicity, ease of implementation, and good performance. Nevertheless, it is observed that there some power losses due to the perturbation, and that it the fails to track the power under fast varying atmospheric conditions [9]-[15]. Perturbation determines the system response and the steady state error. For lower oscillations a small perturb value is required, while large perturb values cause higher oscillations. Unfortunately, smaller perturb values result in a slower response [17]. One solution is to use a perturb value that varies, as proposed by the authors of [18]. The initial perturb value is fixed to be 10% of the open-circuit voltage. Each sequential perturb is 50% of the aforementioned value till the perturb value is 0.5% of the open-circuit voltage. A passable outcome is achieved with this method. However, it depends on the open-circuit voltage, which diverges due to environmental circumstances, and is not so easy to predetermine. The Incremental Conductance (IC) technique works on the principle that the slope of the PV array power curve is zero at the MPP, positive to the left of the MPP, and negative to the right. Likewise, with the P&O technique the increment step size calibrates how quick the MPP is

Manuscript received Apr. 1, 2015; accepted Aug. 14, 2015
Recommended for publication by Associate Editor Hyung-Min Ryu.
[†]Corresponding Author: o.abdelrahim@aswu.edu.eg
Tel: +81-080-2389-9491, Utsunomiya University
[*]Dept. of Electronic and Electrical Eng., Utsunomiya University, Japan

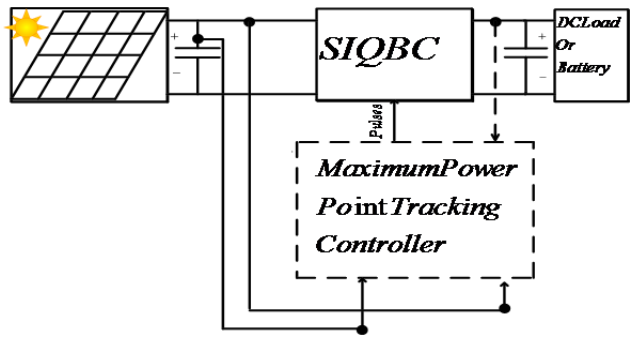

Fig. 1. Configuration of the proposed system.

tracked [16]. Larger increments can lead to faster tracking but might also make the system not operate precisely at the MPP. Instead, it could fluctuate around the MPP. The authors of [19] proposed a short-circuit pulse-based MPPT with a fast scan on the P–V curve to identify the proportional parameter which is used in current-based MPPT [20]. The authors of [21] measure the open-circuit voltage and the short-circuit current, and then the optimum voltage and current values are calculated. Thus, the operating point is progressed with one step to the optimal operating point, according to the computed values.

Finite-set Model Predictive Control (MPC) is a promising control technique [22]-[26]. MPC does not involve any complex control loops. It deliberates the controlled plant as a finite set of linear models, each demonstrating a physical switching state. The controlled variable is predicted in every switching state. The control is assessed and applied at intermediate instants of time [24]-[26]. This results in a variable switching frequency where the maximum switching frequency is limited to half the sampling frequency [22]. Under a variable switching frequency, it is problematic to control Electromagnetic Interference (EMI) and to preserve a desired output voltage quality. Another prediction technique is presented in [22] to uphold a fixed switching frequency without the need for additional on-line calculations.

Hysteresis controllers have been used as a substitute for the Pulse Width Modulation (PWM) technique, due to their essential advantages such as: simplicity in carrying out control operations without complex hardware, fast dynamic response, and inherent capability to bind the peak current injected by the converter [27]-[29]. In conventional hysteresis controllers the error band is generally fixed to a certain value. It is significant that the switching frequency varies within a band [27], [28].

This paper proposes two MPPT techniques for PV applications. The first proposed technique is a two stage algorithm. The two techniques are considered as a modification of the well-known incremental conductance algorithm. The first modification is done by adding a second stage to the incremental conductance algorithm. The second stage is based on the Fixed Frequency Model Predictive Control (FFMPC) MPPT technique. In the second modified technique, the second stage is based on predictive hysteresis. The two proposed techniques are established experimentally. The proposed system under exploration is depicted in Fig. 1. It consists of one PV module, the proposed high-gain SIQBC to boost the low voltage of the PV module to the load voltage level, a dc load or battery, and a schematic of the MPPT controller.

II. Proposed Switched Inductor Quadratic Boost Converter

This paper suggests a transformerless high-gain Switched Inductor Quadratic Boost Converter (SIQBC) for PV applications. Fig. 2 portrays an electrical circuit diagram of the SIQBC. The proposed converter involves four inductors, nine diodes and one switch. The offered converter operates in the Continuous Conduction Mode (CCM). This causes the converter to have two modes of operation.

During the first subinterval when the switch SW is turned on, as shown in Fig. 2(b), diodes D1, D3, D7, D6 and D5 are turned on, and D2, D8 and D4 are turned off. Hence, the two inductors charge in parallel. The characteristic equations of the system are as follows:

$$L_1.\frac{di_{L1}(t)}{dt} = L_2.\frac{di_{L2}(t)}{dt} = v_{pv}(t) - V_d - (R_{on} + R_{L1}).i_{L1}(t) \quad (1)$$

$$i_{pv}(t) = 2i_{L1}(t) \quad (2)$$

$$L_3\frac{di_{L1}(t)}{dt} = L_4\frac{di_{L2}(t)}{dt} = v_{c1}(t) - V_d - (R_{on} + R_{L3}).i_{L3}(t) \quad (3)$$

$$C_o.\frac{dv_o(t)}{dt} = \frac{-V_o}{R} \quad (4)$$

The second mode of operation occurs when the switch SW is off, as shown in Fig. 2(c), diodes D1, D3, D7, D6 and D5 are turned off, and D2, D8 and D4 are turned on. Hence, the two inductors discharge in series. The characteristic equations of the system are as follows:

$$2L_1.\frac{di_{L1}(t)}{dt} = v_{pv}(t) - v_{c1}(t) - 2V_d - 2R_L i_{L1}(t) \quad (5)$$

$$i_{pv}(t) = i_{L1}(t) \quad (6)$$

$$2L_3.\frac{di_{L3}(t)}{dt} = v_{c1}(t) - v_o(t) - 2V_d - 2R_L.i_{L3}(t) \quad (7)$$

$$C_o.\frac{dv_o(t)}{dt} = i_{L3}(t) - \frac{V_o}{R} \quad (8)$$

From equations (1) and (5):

$$V_{pv}.D - V_d.D - (R_{on} + R_{L1}).I_{L1}D + \frac{1}{2}.(1-D).V_{pv}.2d - \frac{1}{2}.(1-D).V_{c1} - (1-D).V_d - (1-D).R_L.I_{L1} = 0 \quad (9)$$

$$V_{c1} = \frac{2}{(1-D)}.\left(V_{pv}.\left(D + \frac{(1-D)}{2}\right) - V_d - I_{L1}.(R_{on}.D + R_{L1})\right) \quad (10)$$

From equation (3) and (7):

$$V_{c1}.D - V_d.D - (R_{on} + R_{L3}).I_{L3}.D + \frac{1}{2}.V_{c1}.(1-D) - \frac{1}{2}.V_o.(1-D) - (1-D).V_d - (1-D).R_{L3}.I_{L3} = 0 \quad (11)$$

$$V_o = \frac{2}{(1-D)}.\left(V_{c1}.\left(D + \frac{(1-D)}{2}\right) - V_d - I_{L3}.(R_{on}.D + R_{L3})\right) \quad (12)$$

The proposed converter has a very high gain. The ideal gain of the proposed converter is given by the following equation:

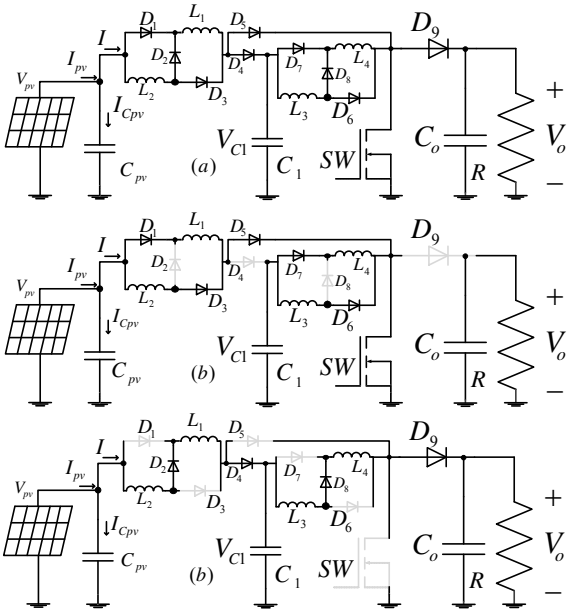

Fig. 2. SIQBC and its modes of operation (b) Mode 1 (c) Mode 2.

$$\mu = \frac{V_o}{V_{in}} = \frac{(1+D)^2}{(1-D)^2} \quad (13)$$

The voltage gain of the Quadratic Boost Converter (QBC) proposed in [30] is given by:

$$\mu = \frac{V_o}{V_{in}} = \frac{1}{(1-D)^2} \quad (14)$$

Meanwhile, the voltage gain of the Switched Inductor Converter (SIC) proposed in [31] is given by:

$$\mu = \frac{V_o}{V_{in}} = \frac{(1+D)}{(1-D)} \quad (15)$$

The voltage gain of the Traditional Boost Converter (TBC) in [32]is given by:

$$\mu = \frac{V_o}{V_{in}} = \frac{1}{(1-D)} \quad (16)$$

Where $L1$, i_{L1}, v_{pv}, v_{c1}, V_d, i_{pv}, $L3$, i_{L3}, v_o, R, R_{on}, R_{L1}, R_{L3}, and C_o refer to inductor L1 inductance, inductor L1 current, PV voltage, capacitor C1 voltage, diode voltage, PV current, inductor L3 inductance, inductor L3 current, output

voltage, load resistance, on resistance of the switch, equivalent series resistance of inductor L1, equivalent series resistance of inductor L3, and output capacitance, respectively.

The proposed SIQBC has a high gain compared to the other transformerless topologies in the literature. Fig. 3 and Fig. 4 depict a gain and efficiency comparison between the proposed SIQBC, Quadratic Boost Converter (QBC), Switched Inductor Converter (SIC), and Traditional Boost Converter (TBC). The efficiency was calculated by considering an input voltage fixed at 30 V. Load resistance is fixed and the following losses of the circuits are taken into account: diode forward voltage drop, switch on resistance and inductor equivalent series resistance. The values of these losses are depicted in Table I. Fig. 3 depicts the ideal voltage gain versus the duty cycle for the proposed SIQBC, SIC, QBC and TBC. Having a higher voltage gain is significant in PV applications, since it enables

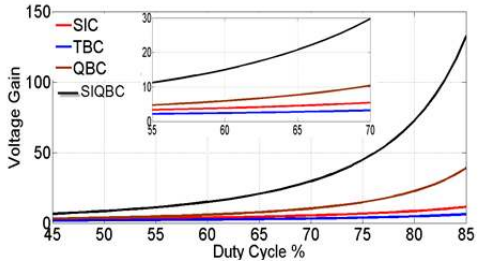

Fig. 3. Ideal voltage gain comparison.

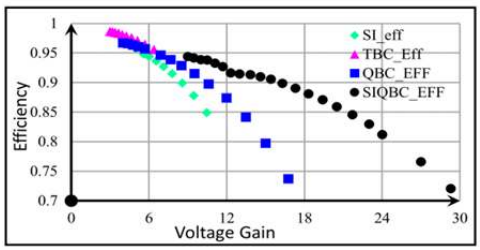

Fig. 4. Calculated efficiency comparison.

the use of a lower number of PV modules. Using fewer PV modules reduces the effect of partial shading. As shown in Fig. 3, the proposed SIQBC has the highest gain among them. Fig. 4 depicts a comparison between the efficiency against the voltage gain of each topology. To compute the efficiency of each converter the following losses were taken into account: diode forward voltage drop, switch on resistance and inductor series resistance. The values of all of the conduction loss parameters are depicted in Table I. According to Fig. 4, at a lower voltage gain, the TBC has the highest efficiency, while at a higher gain, the proposed SIQBC has the highest efficiency. The target of this paper is for ac module applications, which is why high-gain converters are required.

Table II displays the voltage stresses of the proposed SIQBC. As shown in the table, the switch has a reverse voltage equal to the output voltage, diodes D1, D4, and D3 have a reverse voltage equal to the difference between the capacitor C1 voltage and the input voltage, diode D2 has a reverse voltage equal to the input voltage, diodes D6 and D7 have a reverse voltages equal to the difference between the output voltage and the capacitor C1 voltage, diode D8 has a reverse voltage equal to the voltage of capacitor C1, diode D9 has a reverse voltage equal to the output voltage, and diode D5 has a reverse voltage equal to the difference between the output voltage and the input voltage. The voltage stresses of the SIC are also depicted in Table II. As can be seen in the table, the switch has a reverse voltage equal to the output voltage, diodes D1 and D2 have a reverse voltage equal to the difference between the output voltage and the input voltage, diode D3 has a reverse voltage equal to the input voltage, and diode D4 has a reverse voltage equal to the difference between the output voltage and the input voltage. Table II shows the voltage stresses of the TBC. As can be seen in the table, the switch has a reverse voltage equal to the output voltage, and diode D4 has a reverse voltage equal to

TABLE I
PARAMETER USED IN LOSSES CALCULATIONS

Losses item	value
Diode forward voltage drop	.5 V
Switch on resistance	.3 Ω
Inductor series resistance	.034 Ω

TABLE II
COMPONENTS VOLTAGE STRESSES COMPARISON.

Comp.	Reverse voltage	Comp.	Reverse voltage
Proposed SIQBC Components voltage stresses.			
D2	Vin	D1=D3	Vc1-Vin
D8	Vc1	D7=D6	Vo-Vc1
D9	Vo	SW	Vo
D4	Vc1-Vin	D5	Vo-Vin
The SIC components voltage stresses.			
D1=D2	Vo-Vin	SW	Vo
D3	Vin	D4	Vo-Vc1
TBC components stresses.			
D4	Vo-Vc1	SW	Vo
QBC components stresses.			
D2	Vo-Vin	D3	Vo-Vin
D1	Vc1-Vin	SW	Vo
D2	Vo-Vin	D3	Vo-Vin

the difference between the output voltage and the input voltage. Table II shows the voltage stresses of the QBC. As shown in the table, the switch has a reverse voltage equal to the output voltage, diodes D2 and D3 have a reverse voltage equal to the difference between the output voltage and the input voltage, and diode D1 has a reverse voltage equal to the difference between the capacitor C1 voltage and the input voltage.

III. FIXED FREQUENCY MODEL PREDICTIVE MPPT CONTROL

The MPC principle of operation is illustrated graphically in Fig. 5. Fig. 5 clearly illustrates the essential properties of the model predictive control strategy. All of the possible system transitions $y_{Pn}(K+1)$ can be predicted using the discrete-time model of the system for all of the control actions of N (N = 1, 2,3 . . . n). Take N = 1 as an example; the system behavior at the k + 1 instant can be predicted with the measured value y(k) and n possible voltage vectors. This results in n possible values $y_{P1,}\ y_{P2,}\ \ldots\ldots y_{Pn}$.

Suppose that y_{P2} is the closest to y^*. Then, the voltage vector producing y_{P2} will be selected and applied between the k and (k + 1) instants. The MPC for power electronics converters can be designed using the following steps:

1) Model the power converter to identify all of the possible switching states and their relation to the input or output voltages or currents;

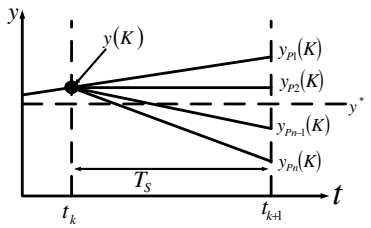

Fig. 5. MPC principle of working.

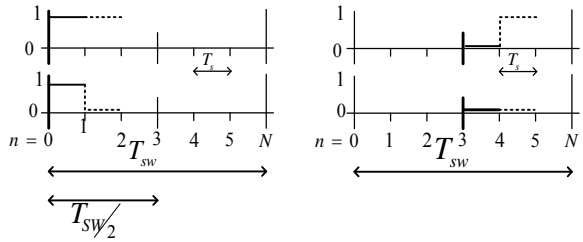

Fig. 6. Depiction of the MPC switching period and prediction possibilities. (a) Predictions when n<N/2. (b) Predictions when n>N/2.

2) Define a cost function that represents the desired behavior of the system;
3) Obtain discrete-time models that make it possible to predict the future behavior of the variables to be controlled.

Predictions of the future values of the controlled variables are required in MPC. Since the target is to control the PV current to extract the maximum amount of power from the PV, the two controlled variables are the PV output voltage and current. Predictions of the future values of the circuit variables gives the advantages of fast reference tracking.

To allow the MPC to operate at a fixed frequency, choose the desired switching frequency with a time period,T_{sw} where the switching period is divided into a number of N steps, and each step represents the sampling period,T_s. The relationship between T_{sw}, N and T_s is as follows:

$$\frac{T_{sw}}{T_s} = N \qquad \text{Where } N \in \{2,4,6 \ldots \ldots\} \qquad (17)$$

Fig. 6 illustrates how the MPC designed to operate at fixed frequency. The operation of fixing the switching frequency of the MPC can be simplified as follows: while n<N/2, the algorithm assumes starting in the on state and predicts whether to stay on or to turn off. The algorithm then generates active states until the optimization process indicates that zero states are required. As a result, zero states remain until n=N/2. For n>=N/2, the algorithm assumes that the system now starts in the off state, and a prediction is made to determine whether the system should stay off or turn on. Once the system is switched on, it will remains on until the end of the switching period. After it has been resettled, the prediction process is restarted for the next switching period. This approach ensures that the system is switched at a fixed switching frequency. A model for the controlled system is necessary to enable predictions of the system variables and selection of the optimum operation

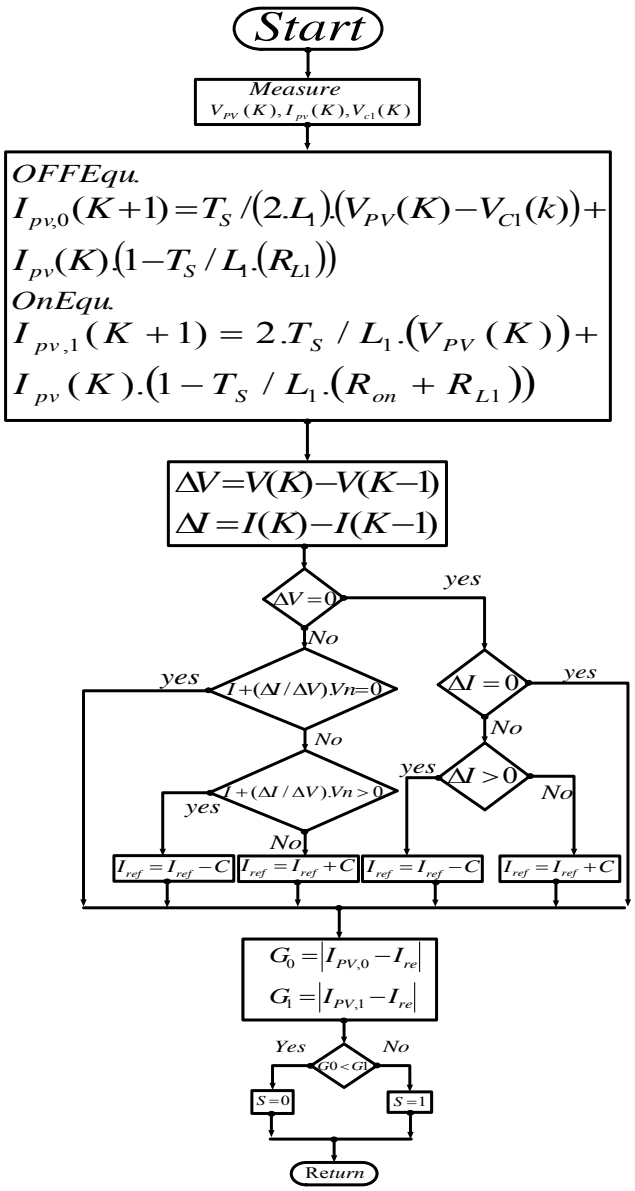

Fig. 7. Flowchart of INC-MPC Algorithm.

according to the specified cost function.

A. Discretization

A model for the controlled system is required for the implementation of the finite-set model predictive control. To construct the model, discretization is required. Discretization of the proposed SIQBC can be done as follows:

$$\text{Let} \quad \frac{di_L(t)}{dt} = \frac{I_L(k+1)-I_L(k)}{T_s} \tag{18}$$

Consider that the sampling time is T_s. As a result, the discretization of the system equations can derive from (1) to (5) discrete equations when the switch SW is on:

$$I_{L1}(k+1) = \frac{T_S}{L1}.\left(V_{pv}(k)-V_d\right)+I_{L1}(K).\left(1-(R_{on}+R_{L1})\right) \tag{19}$$

Replacing the value of $I_{L1}$by its value in equation (2), the following equation can be obtained:

$$I_{pv,1}(k+1) = \frac{2T_S}{L1}.\left(V_{pv}(k)-V_d\right)+I_{pv}(K).\left(1-\frac{T_S}{L1}.(R_{on}+R_{L1})\right) \tag{20}$$

The discrete equation when the switch SW is off:

$$I_{pv,0}(k+1) = \frac{T_S}{2L1}\left(V_{pv}(k)-V_{c1}-2V_d\right)+I_{pv}(K)\left(1-\frac{T_S}{L1}R_{L1}\right) \tag{21}$$

The behavior of the restrained variables can now be predicted for the next sampling instant to obtain the control actions for both the present and a future period. For estimating the prospective behaviors of the monitored variable photovoltaic current, the photovoltaic voltage and converter output voltage are measured.

The key parameter of the MPC is the cost function since it determines the needed control function. In the proposed system, the needed control function is to control the PV's output current and voltage. For the required control criteria of the proposed system, the cost function is given as (22) and (23).

The cost function of this system when a switch is turned off:

$$G_0 = \left|I_{pv,0}(k+1) - I_{ref}\right| \tag{22}$$

The cost function of this system when a switch is turned on:

$$G_1 = \left|I_{pv,1}(k+1) - I_{ref}\right| \tag{23}$$

Where $I_{pv,0}(k+1)$, $I_{pv,1}(k+1)$, I_{ref}, G_0, G_1 and V_{c1} are related to the predicted current of the PV module when the switch is turned off, predicted current of the PV module when the switch is turned on, reference current generated by the IC algorithm, cost function when the switch is turned off, cost function when the switch is turned on, and capacitor C1 voltage, respectively.

A flow chart of the proposed system is depicted in Fig. 7. The operation of the proposed technique is as follows: the current and voltage of the PV module, and output voltage are measured. The prediction of the upcoming value of the PV voltage and current is performed in two states. State one is when the switch is turned on, and state two is when the switch is turned off. The difference between the current values and previous values of the voltage and current of the PV module is calculated afterwards. The algorithm checks the difference in the voltage if it is equal to zero. After that, the difference with the current is checked. If it is equal to zero the algorithm keeps the reference current with no changes. However, if it is greater than zero, the algorithm decreases the reference current; and if it is less than zero, the algorithm increases the reference current. If it is not equal to zero, the algorithm checks the term. If this term is equal to zero the algorithm keeps the reference current with no change. However, if this term is greater than zero, the algorithm decreases the reference current; and if it is less than zero, the algorithm increases the reference current. After generating the reference current, the algorithm calculates both the cost function during the turn on case and the cost function when the switch is turned off. Finally, the algorithm does some

optimization according to the minimum criteria. If it is smaller than the criteria, then the result of the algorithm is to turn off the switch. On the other hand, if it is greater than the criteria, the controller turns on the switch.

IV. Fixed Frequency Predictive Hysteresis Controller

Fig. 8 represents the two stage predictive hysteresis MPPT controller. The photovoltaic voltage and current are measured and used by the IC algorithm to increment or decrement the reference current, which allows the PV module to function at the maximum power. The predictive hysteresis stage matches the measured current and the reference current, which produces the optimum pulses for the converter. The hysteresis band calculation is used to generate the adaptive hysteresis band for fixing the switching frequency. Adding PHC develops the performance of the MPPT control and gives a faster response and the ability to extract maximum power under different environmental conditions.

The development of the PV output current with hysteresis control is depicted in Fig. 9. Fig. 9 depicts the PV output current, the reference current and the adaptive hysteresis band. The difference between the PV output current and the reference current can be expressed as follow:

$$\delta = i_{pv} - i^* \tag{24}$$

Where i_{pv} is related to the output current of the PV module, δ is the difference between the measured and reference current, and i^* is the reference current generated by the IC algorithm.

It is possible to deduct an equation for each of the switching periods according to Fig. 9, for $[0,t_1]$:

$$\frac{d\delta}{dt} = \frac{di_{pv}}{dt} - \frac{di^*}{dt} = \frac{2h}{t_1} \tag{25}$$

And for $[t_1, Ts]$:

$$\frac{d\delta}{dt} = -\frac{di_{pv}}{dt} - \frac{di^*}{dt} = -\frac{2h}{t_2} \tag{26}$$

Bear in mind the equivalent circuit of the proposed SIQBC and use equations (1) and (5). For the sake of simplicity the losses will be deducted from equation (1) and (5).

The PV output current when the switch of the SIQBC is turned on is given by:

$$V_{pv} = L1.\frac{di_{pv}}{dt} \tag{27}$$

While its descriptive equation when the switch is turned off is as follows:

$$V_{pv} - V_{c1} = 2.L.\frac{di_{pv}}{dt} \tag{28}$$

Substituting $\frac{di_{pv}}{dt}$ in equations (27) and (28) by it is value in equations (25) and (26), respectively.

$$V_{pv} = L.\left(\frac{d\delta}{dt} + \frac{di^*}{dt}\right) \tag{29}$$

$$V_{pv} - V_{c1} = 2.L.\left(\frac{d\delta}{dt} + \frac{di^*}{dt}\right) \tag{30}$$

By the substitutions of equations (29) and (30) into equations (25) and (26) it is possible to obtain the following

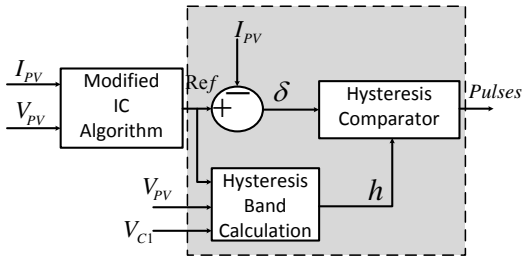

Fig. 8. Proposed Predictive Hysteresis control based Maximum Power Point tracking control.

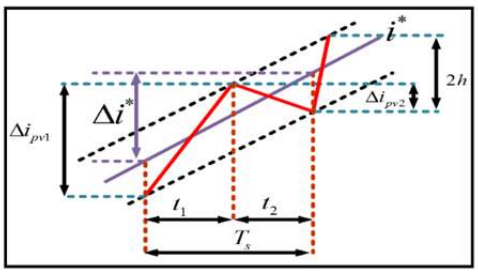

Fig. 9. PV output current with hysteresis control.

equations:

$$\left(V_{pv} - L.\frac{di^*}{dt}\right).t_1 = 2.L.h \tag{31}$$

$$\left(V_{pv} - V_{c1} - 2.L.\frac{di^*}{dt}\right).t_2 = -4.L.h \tag{32}$$

Adding equations (31) and (32):

$$t_2 = \frac{T_s}{(V_{c1}+L.\frac{di^*}{dt})} * \left(V_{pv} - L.\frac{di^*}{dt}\right) + \frac{2.L.h}{(V_{c1}+L.\frac{di^*}{dt})} \tag{33}$$

Finally, by substituting equation (33) into equation (26) and simplifying the terms, equation (34) is reached:

$$h = \frac{-T_s*\left(\frac{V_{pv}}{L} - \frac{di^*}{dt}\right)}{\left(\left(4.L - \frac{2.L}{(V_{c1}+L.\frac{di^*}{dt})}\right).\left(V_{pv} - V_{c1} - 2.L.\frac{di^*}{dt}\right)\right)} * \left(V_{pv} - V_{c1} - 2.L.\frac{di^*}{dt}\right) \tag{34}$$

Equation (34) outlines the adaptive hysteresis band that depends on the system parameters. Where t_1 is the turn on time, t_2 is the turn off time, Ts is the sampling time, L is the inductor value, V_{pv} is the output voltage of the PV, V_o is the converter output voltage, i^* is the reference current, i_{pv} is the output current of the PV module, and h is the adaptive hysteresis band.

V. Experimental Results

In order to authenticate and verify the effectiveness of the proposed techniques, a practical setup is arranged. A schematic of the experimental setup is depicted in Fig. 10. As shown in Fig. 10, a PV simulator is used to simulate the PV module, a prototype of the SIQBC is used as an interface between the dc load and the PV simulator, and a PE Expert with a TI DSP C6713 controller is used to implement the proposed MPPT algorithms. The experimental setup, depicted in Fig. 11, consists of an Agilent E4360A modular solar array simulator to

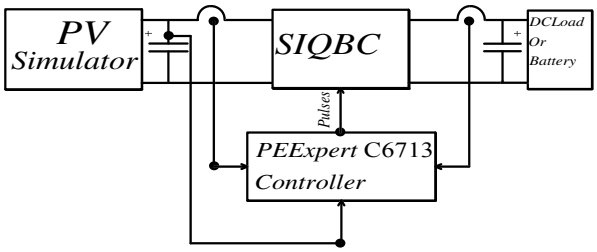

Fig. 10. Schematic of the Experimental Setup.

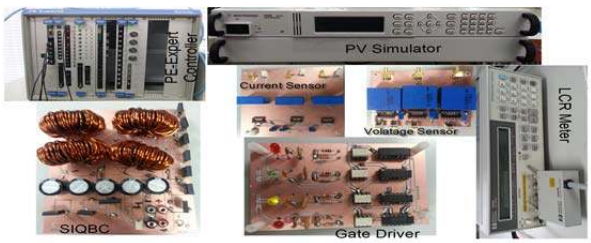

Fig. 11. Experimental Setup.

generate the PV system and the I–V curves. The proposed SIQBC is utilized to boost the output voltage and track the MPP, current sensors are utilized to sense the PV current, and the voltage sensor is utilized to measure the PV output voltage. The PE Expert is a digital controller with a TI DSP C6713 made by my way plus company. The PE Expert C6713 controller is used to realize the proposed MPPT. The circuit of the proposed SIQBC, illustrated in Table III, is built using a IXTK22N100L, an N channel MOSFET, and a VS-EPU3006-N3, fast rectifier diode. The inductor of the circuit is made using a toroid core 0077194A7. For measurement purposes, an LEM LA55-P current sensor and a LEM LV25-P voltage sensor are used.

Different I–V curves are programmed into the PV source simulator to examine the experimental system under different weather conditions. The characteristic of the programmed PV module is depicted in Table IV and the I-V curves are depicted in Fig. 12. For comparison purposes, the IC algorithm is also implemented to compare its performance with that of the proposed MPPT techniques. All of the techniques are designed to operate at a switching frequency equal to 30 KHz, and tested under different environmental conditions. The algorithms are tested under abrupt changes in solar irradiation. The solar radiation changed from 1000 W/m2 to 900 W/m2, and then to 750 W/m2. The result of the IC algorithm is depicted in Fig. 13. In this experiment the solar radiation changed from 1000 W/m2 to 900 W/m2, and then back to 1000 W/m2. The incremental conductance algorithm can track the maximum power. However, as shown in Fig. 13, the algorithm requires about 0.1 S to reach the steady state. The result of applying the proposed MPC-MPPT algorithm is depicted in Fig. 14. The MPC-MPPT algorithm was tested when radiation changed from 1000 W/m2 to 900 W/m2, and then to 750 W/m2. As can be seen from the figure, the MPC-MPPT algorithm is able to track the maximum power with a fast response, since the

TABLE III
CIRCUIT PARAMETERS.

Switching Frequency	30 KHz
L1= L2= L3= L4	2 mH
Sampling time	10 µS
Diode	VS-EPU3006-N3
Switch	IXTK22N100L

TABLE IV
PV MODULE SPECIFICATION.

Short Circuit Current (A)	4.2
Current at MPP (A)	3
Open Circuit Voltage (V)	25
Voltage at MPP (V)	17.8

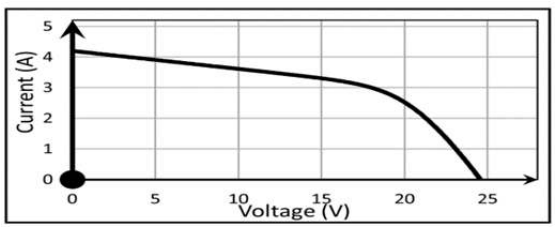

Fig. 12. Programmed PV specifications.

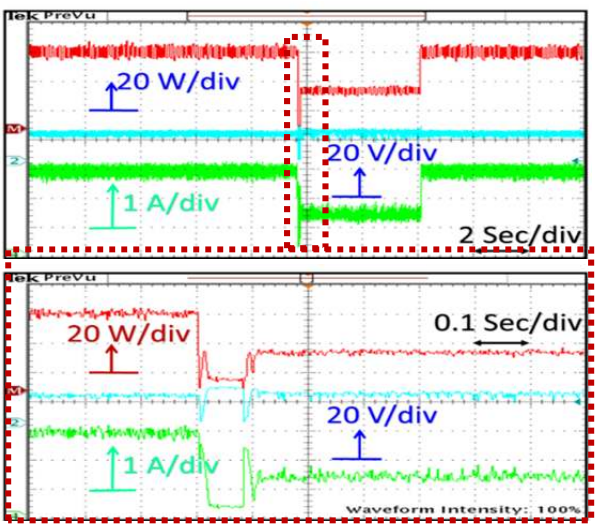

Fig. 13. Incremental Conductance result with reduction in Radiation G from 1000 to 900 to 1000 W/m2.

settling time is around 0.02 S. Finally, the results of applying the predictive hysteresis MPPT are depicted in Fig. 15. The predictive hysteresis controller was tested when the radiation changed from 1000 W/m2 to 900 W/m2, and then to 750 W/m2. The predictive hysteresis controller requires only 0.02 S to reach the steady state and track the maximum power. It can be concluded from these results that both the MPC and Hysteresis based MPPT have a fast response and the ability to track the maximum power point. Meanwhile, the IC algorithm requires a longer time to reach the steady state, and in case of severe changes in environmental conditions, it is not able to track the maximum power.

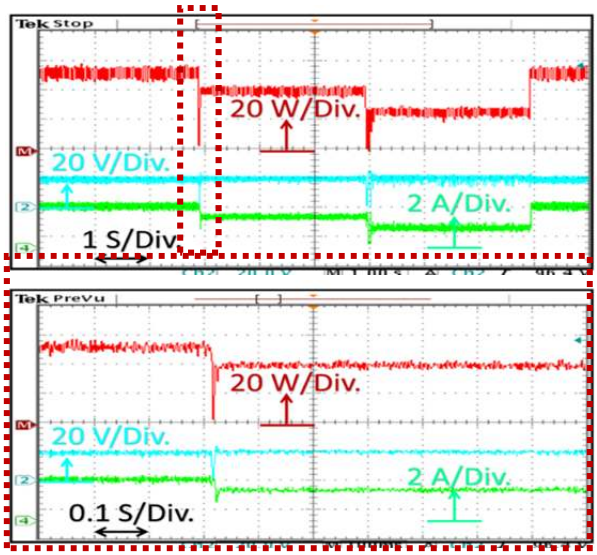

Fig. 14. Proposed MPC-MPPT Technique with reduction in Radiation G from 1000 to 900 to 750 W/m2.

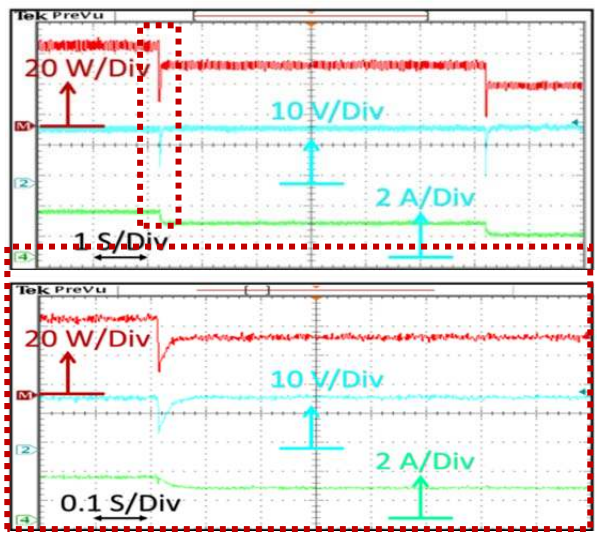

Fig. 15. Proposed Hysteresis MPPT result with reduction in radiation G from 1000 to 900 to 750 W/m2.

The second part of the experimental results are established to compare the proposed SIQBC, SIC, and TBC. Prototypes for the three topologies are built and tested for comparison purposes. The three prototypes are built using IXTK22N100Ls, N channel MOSFETs, VS-EPU3006-N3s, and fast rectifier diodes. The switching frequency is fixed at 30 KHz. The efficiency of the three converters is calculated at different voltage gain points. Fig. 16 is a depiction of the efficiency versus the voltage gain for the three topologies. At low voltage gain application the traditional boost converter is the best choice, since it has the highest efficiency. Unfortunately, in ac module technology a higher voltage gain is required. That is why the TBC is not a good solution for these applications. The proposed SIQBC has the highest efficiency at a high gain. The proposed converter gives a voltage gain higher than 10 times

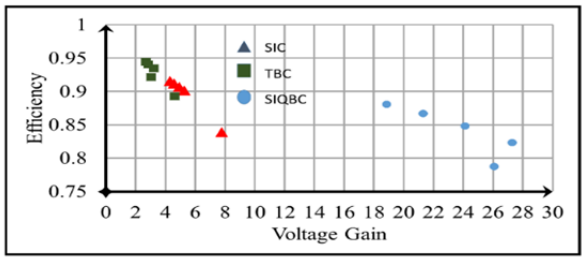

Fig. 16. Measured Efficiency comparison.

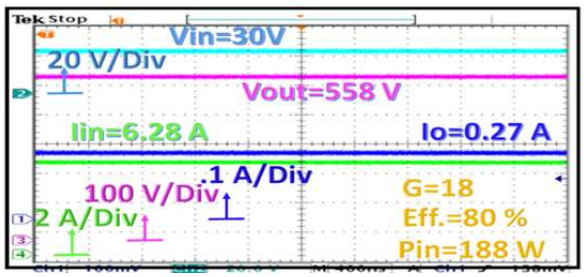

Fig. 17. Quadratic Boost Switched Inductor. (CH1: is the load current, Ch2: is the input voltage, Ch3: is the load voltage and Ch4: is the input current).

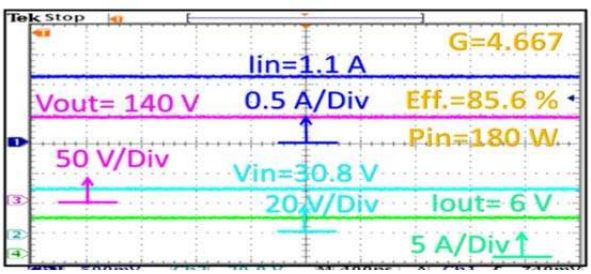

Fig. 18. Switched Inductor Converter. (CH1: is the load current, Ch2: is the input voltage, Ch3: is the load voltage and Ch4: is the input current).

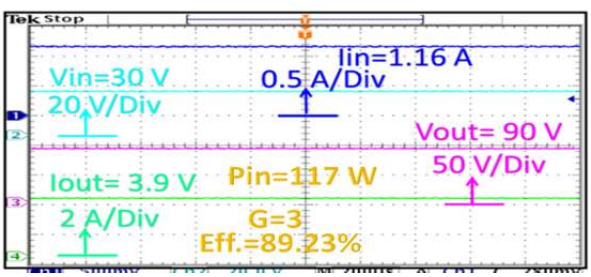

Fig. 19. Traditional Boost Converter. (CH1: is the load current, Ch2: is the input voltage, Ch3: is the load voltage and Ch4: is the input current).

with improved efficiency. From Fig. 16, the proposed SIQBC is the best solution for ac module technology applications. The measured experimental results for the three topologies are depicted in Fig. 16. As can be seen from the graph, the TBC has the highest efficiency among the three. Both the SI and SIQBC have comparative efficiency.

The curve shows that the TBC has the highest efficiency. However, this happens at a low-voltage gain. For higher voltage gains, the proposed SIQBC has the highest efficiency.

A high gain is essential in ac module technology. In the case of ac module technology, only one PV module is connected. This means that the available dc voltage is very small. That is why high-voltage gain converters are necessary. For gain comparison purposes, the three topologies are tested at an input voltage equal to 30 V and a duty cycle equal to 0.7. As depicted in Fig. 17, the proposed SIQBC can produce a 558V output with only a 30V input voltage at a duty cycle of D=.7. The obtained gain is higher than 18 times. The target of this paper is the usage of a lower number of PV modules, which means low power applications. Fig. 18 is the result of the SIC at a duty cycle of D=0.7 and an input voltage of 30 V. Under these conditions the converter produces 140 V. The obtained gain is higher than 4 times. As depicted in Fig. 19, the TBC is tested with a 30V input voltage and a duty cycle that has settled to .7. Under these conditions, the output voltage is about 90 V. The obtained gain is about 3.

VI. Conclusion

This paper presented two MPPT procedures for photovoltaic applications. The first technique is based on the model predictive control, and the second technique is based on the predictive hysteresis control. The two techniques were implemented using a PE expert C6713 controller and compared to the IC algorithm. The proposed systems had the advantages of tracking the maximum power under different environmental conditions. The algorithms were tested with abrupt changes in radiation from 1000 to 900, and then to 750 W/m2. The second part of this paper was the development of a very high gain switched inductor quadratic boost converter. The proposed converter is one solution for AC module technology. An experimental comparison between the proposed converter and other well-known transformerless topologies was presented. The results showed that the proposed SIQBC has the highest gain and the highest efficiency at a high gain.

Acknowledgment

The author would like to thank the Egyptian higher ministry of education for supporting him to complete his study in Japan. This work was supported by JSPS KAKENHI grant number 15K05929.

References

[1] European Photovoltaic Industry Association, "Global market outlook for photovoltaics 2014-2018," available online at: www.epia.org, 2014.

[2] E. koutroulis and F. Blaabjerg, "Overview of maximum power point tracking techniques for photovoltaic energy production systems," *Electric Power Components and Systems*, Vol. 43, No. 12, pp. 1329-1351, Jul. 2015.

[3] O. Abdel-Rahim, M. Orabi, E. Abdelkarim, M. Ahmed, and M. Z. Youssef, "Switched inductor boost converter for PV applications," in *Proc. APEC 27*, pp. 2100-2106, 2012.

[4] O. Abdel-Rahim, M. Orabi, and M. E. Ahmed, "High gain single-stage inverter for photovoltaic AC modules," in *Proc. APEC 26*, pp. 1961-1967, 2011.

[5] O. Abdel-Rahim, M. Orabi, and M. E. Ahmed, "Development of high-gain high-efficiency grid-connected inverter for PV Module," in *Proc. PEDG 2*, pp. 368-373, 2010.

[6] M. Liserre, T. Sauter, and J. Y. Hung, "Future energy systems: integrating renewable energy sources into the smart power grid through industrial electronics," *IEEE Ind. Electron. Mag*., Vol. 4, No. 1, pp. 18-37, Mar. 2010.

[7] T. Senjyu, T. Shirasawa, and K. Uezato, "A maximum power point tracking control for photovoltaic array without voltage senso," *Journal of Power Electronics*, Vol. 2, No. 3, pp.155-161, Jul. 2002.

[8] H. Bae, J. Park, B. Cho, and G. Yu, "new MPPT control strategy for two-stage grid-connected photovoltaic power conditioning system," *Journal of Power Electronics*, Vol. 7, No. 2, pp.174-180, Apr. 2007.

[9] S. Thangaprakash, "Unified MPPT control strategy for z-source inverter based photovoltaic power conversion systems," *Journal of Power Electronics*, Vol. 12, No. 1, pp. 172-180, Jan. 2012.

[10] M. Momayyezan and H. Iman-Eini, "Developed MPPT algorithm for photovoltaic systems without a voltage sensor," *Journal of Power Electronics*, Vol. 13, No. 6, pp. 1042-1050, Nov. 2013.

[11] K. Ding, X. Wang, Q. Zhai, J. Xu, J. Zhang, and H. Liu "Improved global maximum power point tracking method based on voltage interval for PV array under partially shaded conditions" *Journal of Power Electronics*, Vol. 14, No. 4, pp. 722-732, Jul. 2014.

[12] J. Lee, J. Lee, and K. Lee, "Current sensorless MPPT control method for dual-mode PV module-type interleaved flyback inverters," *Journal of Power Electronics*, Vol. 15, No. 1, pp. 54-64, Jan. 2015.

[13] M. Orabi, M. Ahmed, and O. Abdel-Rahim, "A single-stage high boosting ratio converter for grid-connected photovoltaic systems," *Electr. Power Components Syst*., Vol. 41, No. 9, pp. 896-911, Jul. 2013.

[14] A. Abdelsalam, A. Massoud, S. Ahmed, and P. Enjeti, "High-performance adaptive perturb and observe MPPT technique for photovoltaic-based microgrids," *IEEE Trans. Power Electron*., Vol. 26, No. 4, pp. 1010-1021, Apr. 2011.

[15] G. Carannante, C. Fraddanno, M. Pagano, and L. Piegari, "Experimental performance of MPPT algorithm for photovoltaic sources subject to inhomogeneous insolation," *IEEE Trans. Ind. Electron*., Vol. 56, No. 11, pp. 4374-4380, Nov. 2009.

[16] T. Esram and P. L. Chapman, "Comparison of photovoltaic array maximum power point tracking techniques," *IEEE Trans. Energy Convers*., Vol. 22, No. 2, pp. 439-449, Jun. 2007.

[17] T. Yao and R. Ayyanar, "Maximum-voltage-unit-guided MPPT algorithm for improved performance under partial shading," in *Proc. ECCE05*, pp. 2428-2434, Sep. 2013.

[18] A. Al-Amoudi and L. Zhang, "Optimal control of a grid-connected PV system for maximum power point tracking and unity power factor," in *Proc. PEDS07*, pp. 80-8, Sep. 1998.

[19] T. Noguchi, S. Togashi, and R. Nakamoto, "Short-current

pulse-based maximum-power-point tracking method for multiple photovoltaic-and converter module system," *IEEE Trans. Ind. Electron*., Vol. 49, No. 1, pp. 217-223, Feb. 2002.
[20] M. A. S. Masoum, H. Dehbonei, and E. F. Fuchs, "Theoretical and experimental analyses of photovoltaic systems with voltage and current-based maximum power-point tracking," *IEEE Trans. Energy Convers*., Vol. 17, No. 4, pp. 514-522, Dec. 2002.
[21] S. Kazmi, H. Goto, O. Ichinokura, and H.-J. Guo, "An improved and very efficient MPPT controller for PV systems subjected to rapidly varying atmospheric conditions and partial shading," in *Proc. AUPEC*, pp. 1-6, 2009.
[22] M. Tomlinson, T. Mouton, R. Kennely and P. Stolze, "Model predictive control with a fixed switching frequency for an AC-to-AC converter," in Proc. ICIT 13, Pp. 570-575, Feb. 2013.
[23] O. Abdel-Rahim and H. Funato, "Model predictive control based maximum power point tracking technique applied to ultra step-up boost converter for PV applications," in *Proc. ISGT ASIA*, pp. 138-142, May 2014.
[24] O. Abdel-Rahim and H. Funato, "A novel model predictive control for high gain switched inductor power conditioning system for photovoltaic applications," in *Proc. ISGT ASIA*, pp. 170-174, May 2014.
[25] O. Abdel-rahim, H. Abu-Rub, A. Iqbal, and A. Kouzou, "Five-to-three phase direct matrix converter with model predictive control," in *Proc. Power Eng. 13*, pp. 13-17, 2013.
[26] O. Abdel-Rahim and H. Funato, "Modified maximum power point tracking technique based on fixed frequency model predictive control for pv applications," in *Proc. IECON 14*, pp. 5120-5124, 2014.
[27] F. Blaabjerg, R. Teodorescu, M. Liserre, and A. Timbus, "Overview of control and grid synchronization for distributed power generation systems," IEEE Trans. Ind. Electron., Vol. 53, No. 5, pp. 1398-1409, Oct. 2006.
[28] A. Arancibia, K. Strunz, and F. David, "A unified single- and three-phase control for grid connected electric vehicles," IEEE Trans. Smart Grid, Vol. 4, No. 4, pp. 1780-1790, Dec. 2013.
[29] O. Abdel-Rahim and H. Funato, "Novel fixed frequency predictive hysteresis maximum power point tracking control for photovoltaic applications," in *Proc. ICPE 13*, pp. 1897-1901, Jun. 2015.
[30] O. Santos, L. Salamero, G. Garcia, H. Blavi, and D. Mercuri, "Efficiency analysis of a sliding-mode controlled quadratic boost converter," *IET Power Electron*., Vol. 6, No. 2, pp. 364-373, Feb. 2013.
[31] M. E. Ahmed, M. Orabi, and O. Abdel-Rahim, "Two-Stage micro-grid inverter with high voltage gain for PV applications," *IET Power Electron*., Vol. 6, No. 9, pp. 1812-1821, Nov. 2013.
[32] R. W. Erickson and D. Maksimovic, *Fundamental of Power Electronics*, New York, Kluwer Academic Publishers, pp. 187-204, 2004.

Omar Abdel-Rahim received his B.S. and M.S. degrees in Electrical Engineering, from the Faculty of Engineering, Aswan University, Aswan, Egypt, in 2009 and 2012, respectively. He is presently working towards his Ph.D. in the Department Of Electrical Engineering, Utsunomiya University, Utsunomiya, Japan. From 2009-2012, he was a Research Assistant with the Aswan Power Electronic Application Research Center (APEARC) Aswan, Egypt. Since 2010, he has been an Assistant Lecturer in the Department of Electrical Engineering, Aswan University. In 2012, he joined the Texas A&M University at Qatar as a Research Associate. He has authored or coauthored over 20 papers in leading international conferences and journals, mainly on the topics of grid connected inverters and multiphase matrix converters. His current research interests include multiphase machines drives, predictive control, renewable energy, smartgrids, and DC-AC converters.

Hirohito Funato was born on February 26, 1964, in Fukushima, Japan. He received his B.S., M.S., and Ph.D. degrees in Electrical Engineering from Yokohama National University, Yokohama, Japan, in 1987, 1989, and 1995, respectively. He worked at the Tokyo Electric Power Company from 1989 to 1991. He joined the Faculty of Engineering, Utsunomiya University, Utsunomiya, Japan, in 1995, where he is presently working as a Professor. His current research interests include applications of power electronics to power systems, digital control of power electronic circuits, renewable energy, etc. He received a PCC2007 Best Paper Award in 2007, and IEEJ Paper Presentation Awards in 1994 and 1997. Dr. Funato is a member of the IEEJ, IEEE PELS, IAS and IES.

Junnosuke Haruna was born in Hokkaido, Japan, in 1983. He received his B.S., M.S., and Ph.D. degrees in Electrical Engineering from Nagaoka University of Technology, Nagaoka, Japan, in 2006, 2008, and 2011, respectively. He joined the Department of Electrical Engineering, Faculty of Science and Technology, Tokyo University of Science, Noda, Japan, as an Assistant Professor, in 2011. He has been with Utsunomiya University, Utsunomiya, Japan, as an Assistant Professor, since 2014. His current research interests include power electronics, motor control, and electric vehicles. He is a Member of the Institute of Electrical Engineers of Japan, and a Member of IEEE.